

Article

# Exploring the Potential of Sr<sup>2+</sup> for Improving the Post-Hardening Strength and Durability Characteristics of Cement Paste Composites

Byoung Hooi Cho 

Department of Civil Engineering, Sangmyung University, 31 Sangmyeongdae-gil, Cheonan-si 31066, Republic of Korea; byoungcho@smu.ac.kr

**Abstract:** This study investigates the effects of strontium ions on enhancing the post-hardening strength and durability characteristics of hydrated cement composites, exploring their potential use as a rehabilitation method for aging concrete structures. A 30% strontium nitrate solution served as the source of strontium ions. Cement paste specimens with a water-to-cement ratio of 0.5, cured for 28 days, were submerged in the 30% strontium nitrate solution to facilitate strontium ion penetration. Compressive and flexural strength tests were conducted on the specimens and compared to those cured in deionized water. Moreover, the durability performance, including surface abrasion resistance, water sorptivity, and porosity, was examined. Scanning electron microscopy (SEM), energy-dispersive spectroscopy (EDS), and X-ray diffractometry (XRD) analyses were also carried out to investigate the microscopic morphology and chemical characteristics of the specimens. Results indicated that the strontium-treated specimens exhibited notable enhancements in both compressive and flexural strengths, especially in flexural strength. The specimens also demonstrated improved surface abrasion resistance, decreased water absorption, and a marked reduction in porosity. SEM analysis revealed a densified microstructure in the strontium-treated cement paste specimens, and EDS and XRD analyses showed changes in their morphology and chemical compositions and structures, indicating the formation of new types of hydrates. Accordingly, this study suggests that the strontium ion treatment method has significant potential for the maintenance and restoration of aging cementitious materials.

**Keywords:** strontium ion; post-hardening properties; strength and durability; surface abrasion resistance; water sorptivity; porosity



**Citation:** Cho, B.H. Exploring the Potential of Sr<sup>2+</sup> for Improving the Post-Hardening Strength and Durability Characteristics of Cement Paste Composites. *Appl. Sci.* **2024**, *14*, 1841. <https://doi.org/10.3390/app14051841>

Academic Editors: Daniel Ferrández Vega and Alexander Martín Garín

Received: 31 January 2024

Revised: 18 February 2024

Accepted: 22 February 2024

Published: 23 February 2024



**Copyright:** © 2024 by the author. Licensee MDPI, Basel, Switzerland. This article is an open access article distributed under the terms and conditions of the Creative Commons Attribution (CC BY) license (<https://creativecommons.org/licenses/by/4.0/>).

## 1. Introduction

Hydrated cement composites, such as cement concrete, are known for their excellent mechanical properties, including high compressive strength and modulus of elasticity. They have long been established as crucial materials in the modern construction industry, owing to their proven durability over extended periods. However, when continuously exposed to physically harsh conditions, such as repetitive loading, or chemically harsh conditions, like de-icing salt application and exposure to coastal environments, these cement-based composites can begin to deteriorate. This deterioration typically begins at the surface and progresses internally. Acid specifically interacts with the calcium in hydrated cement composites to form calcium chloride (CaCl<sub>2</sub>), a soluble salt. This salt can be leached out, resulting in mass loss and compromising structural integrity. Furthermore, silica gel, a byproduct of the acid reaction, leads to significant physical alterations, leading to the severe degradation of the microstructure [1]. Such deterioration not only impairs material performance but can also reduce the structural integrity and lifespan of structures [2]. Consequently, maintaining concrete infrastructures remains a significant issue in the contemporary construction industry. Road pavements, in particular, being directly subjected to vehicle loads, demand high maintenance. Surface treatment methods, employed for road pavement maintenance, are widely used to enhance durability by improving resistance

to surface abrasion and water ingress, offering a straightforward approach to construction [3,4]. While some studies in asphalt pavement have explored the influence of these surface treatments [5,6], research on their effects on the strength and durability of concrete pavements is still insufficient. However, there have been studies on the impact of these treatments on the safety and rideability of concrete pavements [7,8].

Concrete surface treatment methods are commonly utilized to modify the material properties of hydrated cement composites at the surface and to a certain depth below. This enhances resistance to physical and chemical environmental exposures. These techniques are generally categorized into four types: surface coating, hydrophobic material impregnation, pore-blocking, and multifunctional treatment methods. Among these, the surface coating method, which employs materials like epoxy resin, acrylic, and polymer cementitious materials to create a physical barrier on the surface, is widely used to resist chemical attacks caused by water penetration [9,10]. The hydrophobic impregnation technique renders the concrete surface and the adjacent subsurface layers water-repellent, effectively repelling water and detrimental ions from the cement or concrete matrix. Silane ( $\text{SiH}_4$ ), siloxane ( $\text{Si-O-Si}$ ), and compounds containing these functional groups are primarily used in this hydrophobic impregnation process [11]. Additionally, the pore-blocking method improves the chemical properties of cement hydrates near the surface of concrete infrastructures, such as buildings, bridges, and highways. This is achieved by applying a silicate-based liquid-type permeable material, such as sodium silicate ( $\text{Na}_2\text{SiO}_3$ ) and lithium silicate ( $\text{Li}_2\text{SiO}_3$ ) solutions. These solutions react with calcium hydroxide (CH) in hydrated cement composites to form additional insoluble amorphous calcium silicate hydrate (C-S-H), filling the pores up to a certain depth near the surface. This mechanism enhances durability by improving resistance to water penetration, carbonation, and surface abrasion [12,13]. However, when using supplementary cementitious materials such as fly ash, the amount of calcium hydroxide (CH) initially formed is small [14], and the CH content gradually decreases due to carbonation over time [15]. Therefore, it is difficult to expect the desired effect from the silicate-based treatment solutions on actual aging concrete. It is important to note that such surface treatment methods are unlikely to restore or enhance the strength of concrete components, and the research in this specific aspect has been limited.

Strontium (Sr), classified as an alkaline earth metal, exhibits chemical characteristics that are similar to calcium (Ca). Calcium is notably a primary and abundant component in hydrated cement composites. However, strontium is characterized by its larger chemical reactivity and ionic size compared to calcium ( $\text{Sr}^{2+}$ : 1.13Å vs.  $\text{Ca}^{2+}$ : 0.99Å). Owing to these properties, it is understood that calcium ions can be easily replaced by strontium ions, with the size difference between the two elements leading to a denser microstructure [16,17]. Based on this principle, the research in the medical field is being conducted on osteoporosis treatments and implant materials using strontium to improve bone density through microstructural modification [18–21]. Strontium ions are known to react with cement hydrates in aqueous solutions in three different ways: first, by electrostatic adsorption to C-S-H [22,23]; second, through a  $\text{Ca}^{2+}$ - $\text{Sr}^{2+}$  ion exchange process [24,25]; and third, by forming a strong bond with cement hydrates containing aluminum, such as AFt (ettringite) and AFm (monosulfoaluminate) [26]. Based on this understanding, substituting calcium ions in hydrated cement composites with strontium ions can theoretically reduce the microstructure's porosity, leading to a denser structure with improved resistance to water penetration and overall enhancement of durability performance. This hypothesis underpins recent preliminary research into a permeable surface treatment method using strontium cation ( $\text{Sr}^{2+}$ ), which has shown significant results in improving surface abrasion resistance and water absorption resistance [27]. Building on this background, this study posits that the use of strontium cation-based permeable surface treatment techniques can alter the strength characteristics of already hardened hydrated cement composites in the near-surface region. While similar research was conducted in the past [28], it had limitations in terms of its experimental scope and result analysis.

In this study, the potential of strontium cations as a method for enhancing the durability performance of hydrated cement composites was explored. The cement paste specimens were prepared and treated with strontium cations in solution, and modifications in durability characteristics, such as surface abrasion resistance, water sorptivity, and void content ratio (porosity), were experimentally investigated. Furthermore, special attention was provided to experimentally assessing the potential for improvements in compressive and flexural strength characteristics due to the surface treatment with strontium cations. For the strength tests, the digital image correlation (DIC) technique was utilized to analyze the behavioral characteristics of the specimens. For all test results, *t*-test analyses were performed to identify the significance of the difference in mean values between the Sr<sup>2+</sup> treated group and the untreated group. In addition, changes in the microscopic morphology and chemical compositions and structures of the cement hydrates, induced by the strontium ions, were observed through analyses conducted using a scanning electron microscope (SEM), an energy-dispersive spectrometer (EDS), and X-ray diffractometer (XRD).

## 2. Experimental Section

### 2.1. Materials and Specimens

#### 2.1.1. Source of Strontium Cation

Strontium nitrate (Sr(NO<sub>3</sub>)<sub>2</sub>) powder was employed in this study as a source of strontium cations. Strontium nitrate is an inorganic compound that consists of strontium ions (Sr<sup>2+</sup>) and nitrate ions (NO<sub>3</sub><sup>-</sup>), characterized by its white crystalline solid form and high solubility in water (see Figure 1). In this study, 30% strontium nitrate aqueous solution was prepared by dissolving the powder in deionized water using a 3:7 weight ratio, at room temperature (24 °C). This concentration ensures no precipitation, maintaining consistency for the experiments.

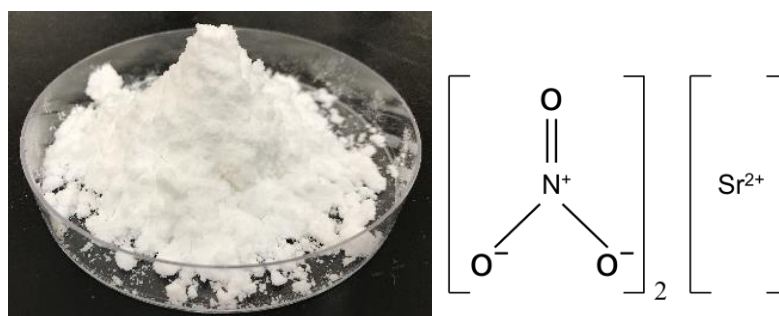


**Figure 1.** Strontium nitrate powder and schematic chemical structure.

#### 2.1.2. Specimen Preparation

Specimens were prepared by mixing cement paste with a water-to-cement ratio (*w/c*) of 0.5. The composition of the ordinary Portland cement (OPC) used in this study is presented in Table 1 and conforms to the standards of the American Society for Testing and Materials (ASTM) C150 [29].

**Table 1.** Chemical composition of OPC (Type I).

Component	SiO <sub>2</sub>	CaO	Al <sub>2</sub> O <sub>3</sub>	SO <sub>3</sub>	Fe <sub>2</sub> O <sub>3</sub>	IR <sup>(1)</sup>	LOI <sup>(2)</sup>
Percentage (%)	21.5	64.9	4.2	0.7	3.5	1.1	-

<sup>(1)</sup> Insoluble residue; <sup>(2)</sup> Loss of ignition.

Cement paste specimens were prepared for conducting various tests: cubic specimens (50 × 50 × 50 mm) for the compressive strength test, prism specimens (30 × 40 × 200 mm) for the flexural strength test, disc specimens (φ100 × 10 mm) for the surface abrasion resistance test, and additional disc specimens (φ100 × 50 mm) for water sorptivity and

porosity measurements. Initially, the fabricated specimens were cured in a water bath for the first 28 days. Subsequently, the specimens were transferred to an environmental chamber and dried for 48 h at a temperature of 40 °C and a relative humidity of 40%. Following this, the specimens were divided into six groups as described in Table 2 for a specified additional curing process. The first group of specimens (S1) was additionally cured in a 30% strontium nitrate solution for 24 h (1 day), while the second and third groups included specimens (S3 and S7) that were additionally cured for 3 and 7 days, respectively. To compare the experimental results with these groups cured in a 30% strontium nitrate solution, a set of specimen groups (H1, H3, and H7) that underwent additional curing in deionized water for the same periods was prepared. For the compressive and flexural strength tests, six specimens were prepared for each condition, and for surface abrasion resistance, water sorptivity, and porosity measurements, three specimens were prepared for each condition.

**Table 2.** Specimen IDs.

Solutions for Additional Curing	Period of Additional Curing (Day)		
	1	3	7
In 30% Sr(NO <sub>3</sub> ) <sub>2</sub>	S1	S3	S7
In deionized water	H1	H3	H7

## 2.2. Test Methods

### 2.2.1. Mechanical Strength Tests

To investigate the modifications in strength characteristics of specimens additionally cured in a 30% strontium nitrate solution for 1, 3, and 7 days, compared to those cured in deionized water for the same periods, tests for compressive and flexural strength were conducted. The compressive strength test was performed on cube specimens in accordance with ASTM C109 [30]. For this test, a Universal Testing Machine (UTM) (HD-201) (Hyundai Precision Industry Co., Ltd., Seoul, Republic of Korea) was used as the load application device. The specimens were loaded at a rate of 900 N/sec until failure, and the load history was automatically recorded through a connected computer system. The maximum load recorded was then divided by the cross-sectional area to calculate the compressive strength. For the flexural strength, the three-point loading test method, as per ASTM C293 [31], was employed. The span length between supports was set at 150 mm, and the test was conducted using a UTM at a displacement rate of 0.005 mm/min. Since the load at fracture in the flexural strength test is not very high, a precise measurement was ensured in this study by using a separate load cell (DBHS-1t) to record load history. The flexural strength ( $f$ ) was calculated using the load at the point of fracture with the following formula:

$$f = \frac{3PL}{2bd^2} \quad (1)$$

where  $f$  = flexural strength (MPa);  $P$  = applied load (N);  $L$  = span length (mm);  $b$  = width of specimen (mm); and  $d$  = depth of specimen (mm).

### 2.2.2. Digital Image Correlation (DIC)

In this study, the DIC technique was utilized to analyze the behavioral characteristics during strength tests. DIC is a non-contact method that measures displacement and strain by contrasting digital images of a specimen's surface before and after deformation. To facilitate this, a surface with significant contrast was created using black and white matte spray to form a random pattern, as shown in Figure 2a. Images of the specimen before and after deformation were captured by a CCD (charge-coupled device) camera, with the movement of these patterns in small areas being tracked to measure displacement and strain. In the initial, undeformed reference image, multiple pixels were designated as a small subset, and their transformation was calculated by contrasting them with their

deformed subset in the post-deformation image [32]. Each pixel within this region has a unique luminance, allowing for the displacement of the central point of a region with a specific brightness in the pre-deformation image to be measured. The displacement of an arbitrary point nearby was then measured, correcting for the deformed area. This process of aligning the positions of each subset in the reference and deformed images provides information on displacement and strain.

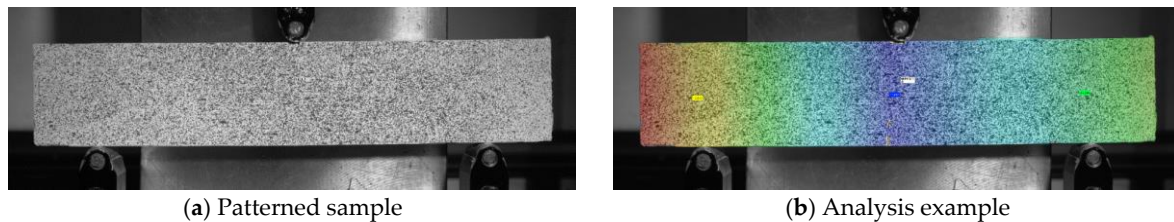


**Figure 2.** DIC.

During the compressive and flexural strength tests, load was applied by the UTM while the DIC system was used to measure the specimen's strain and displacement. Figure 2b illustrates an example of DIC analysis during flexural strength test. For the compressive strength test, the strain in the x-x direction ( $\epsilon_{xx}$ ) was measured, while for the flexural strength test, the relative deflection at the center of the specimen between two support points ( $\delta_y$ ) was measured. Digital images were captured by the DIC system at a rate of 20 Hz during loading, and subsequent analysis of strain and displacement was conducted using specialized software. This allowed for selective post-experimental analysis of various displacement and strain information at desired locations. For this study, the ARAMIC MC 2D model from OMAGOM, Braunschweig, Germany was used to capture digital images, and GOM SNAP 2D software was employed for displacement and strain analysis.

### 2.2.3. Durability Performance Tests

The evaluation of specimen's surface abrasion resistance was conducted via a Taber Abrasion Tester, as depicted in Figure 3a by following the ASTM D4060. Commencing with an initial weight measurement, specimens were secured onto the tester's platform and subjected to a rotational abrasion at a rate of 60 revolutions per minute under an applied load of 9.8 N. The abrasion was sustained for a period of five minutes for each specimen. Following this process, the specimens were removed, and their post-abrasion weight was meticulously determined to assess weight loss. The loss is indicative of the material's ability to withstand surface abrasion, with a lower weight loss correlating to enhanced abrasion resistance. The weight was gauged using a highly precise scale with the capability to discern weight variations up to an accuracy of  $\pm 0.01$  g.

In parallel, the water absorption rate of the specimens was gauged to assess their sorptivity, pursuant to ASTM C1585 [33]. Four disk specimens for the six specimen IDs were prepared for the water sorptivity evaluation. The arrangement for this assessment is illustrated in Figure 3b. The specimens were coated with a latex polymer paint, barring the bottom surface, to ensure waterproofing. Following the application of the paint, the specimens were left to dry in an environmental chamber, set at an ambient temperature of 24 °C with a relative humidity of 45%, for three days. For the water absorption test, the specimens were positioned with the unsealed surface facing downward on aluminum rod supports, and water was added to a depth of  $2 \pm 1$  mm from the bottom surface. The specimens' weight was recorded at predetermined intervals from the initial water contact for up to 10 days. The cumulative weight change was then calculated to quantify the water sorptivity of each specimen.

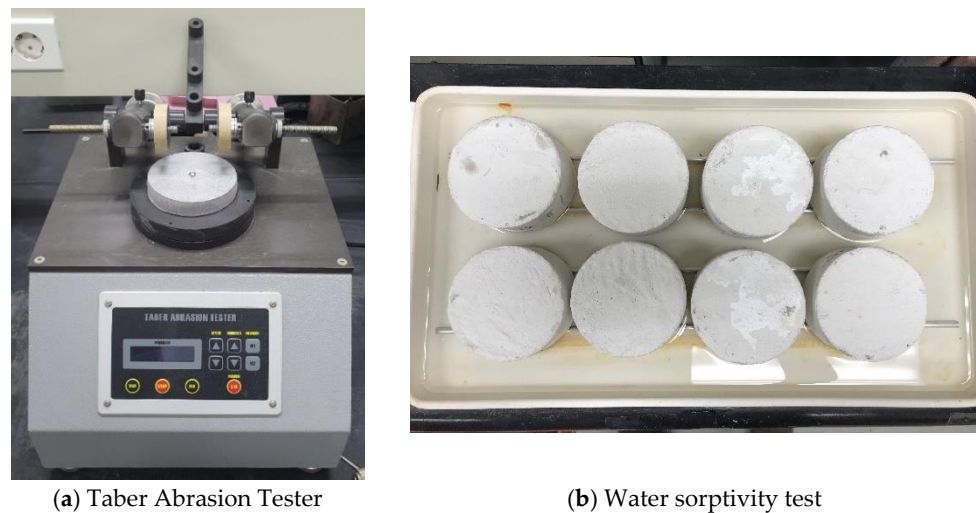


Figure 3. Test setup.

The porosity of the hardened cement paste specimens was determined in accordance with ASTM C1754 [34]. Initially, the weight of the specimens in a fully dried condition was recorded, referred to as  $W_{OD}$ . The specimens were then submerged in deionized water and left until the samples reached full saturation, a state confirmed by monitoring weight change. Following saturation, the weight of the specimens while submerged was documented, denoted as  $W_{Water}$ . Additionally, the mass of the specimens in a saturated surface dry (SSD) condition was ascertained, labeled as  $W_{SSD}$ . Utilizing these measurements, the porosity within the specimens was calculated using the subsequent equation:

$$Porosity = \frac{W_{SSD} - W_{OD}}{W_{SSD} - W_{Water}} \quad (2)$$

### 3. Results and Discussion

#### 3.1. Strengths Characteristics

Figure 4a,b represent the results of the compressive and flexural strength tests for each specimen ID, respectively, including statistical analysis results such as average (Avg.), standard deviation (Std.), and  $p$ -values from  $t$ -test results. It was observed that specimens additionally cured in the 30% strontium nitrate solution exhibited improved compressive and flexural strengths compared to those cured in water for the same period. For compressive strength, the H1 specimen showed 24.25 MPa, while S1 exhibited a higher value of 27.98 MPa, which is approximately 15.4% greater. The compressive strength of S3 was 28.67 MPa, which is about 13.3% higher than the 25.31 MPa of H3. After 7 days of treatment with the strontium nitrate solution, S7 showed a compressive strength of 29.13 MPa, which is about 9.3% higher than H7 (26.66 MPa). Based on the results of the F-test for H groups and S groups, the two groups were assumed to have equal variances, and a  $t$ -test was conducted accordingly. For the results of the compressive strength tests, in the case of H3 and S3, the  $p$ -value was 0.0785, indicating a confidence level of approximately 92%. However, for 'H1 and S1' as well as 'H7 and S7', the  $p$ -values were significantly lower, suggesting that the differences in mean values are highly significant. The strength increase due to the strontium nitrate solution treatment was more pronounced in flexural strength than in compressive strength. The flexural strength of S1 was 7.932 MPa, which is approximately 73.0% higher than the 4.584 MPa of H1. For S3, a value of 8.684 MPa was measured, which is about 73.8% greater than the 4.824 MPa of H3. The flexural strength of S7 was 8.683 MPa, which is about 65.7% higher than the 5.240 MPa of H7. For the flexural strength tests, the  $t$ -test analysis results indicate a high level of confidence in the difference in mean values between the two groups. While specimens additionally cured in deionized water did not show a significant increase in strength within the error range over the 7-day treatment

period, those cured in the strontium nitrate solution demonstrated considerable strength enhancement, especially in the early stages of the treatment.

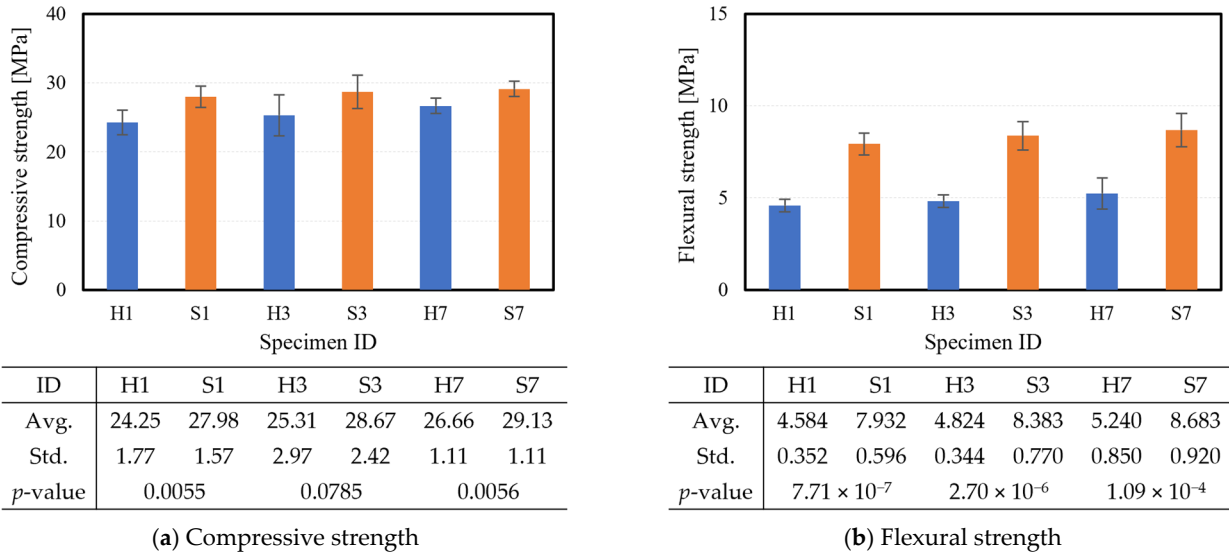


Figure 4. Results of strength tests.

Figure 5a,b show the cross-sections of the flexural strength specimens S1 and S7, respectively. The penetration of the 30% strontium nitrate solution through the surface of the specimens can be clearly observed. The penetration depth was measured to be approximately 2.5–5.0 mm for the S1 specimen, which was immersed for a shorter duration, and about 3.5–6.5 mm for the S7 specimen, which was immersed in the strontium nitrate solution for 6 days longer than S1. Despite this extended immersion, the increase in penetration depth was only in the range of 1.0–1.5 mm, suggesting that most of the penetration occurs during the early stage of immersion. This observation likely explains the more significant increase in compressive and flexural strengths observed in the early stages of the treatment.

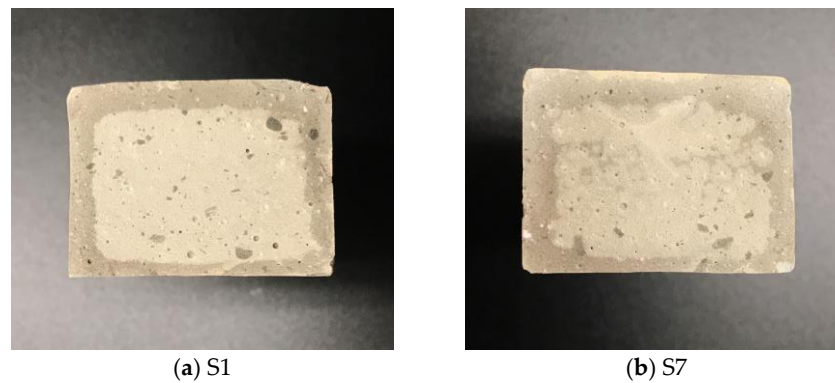
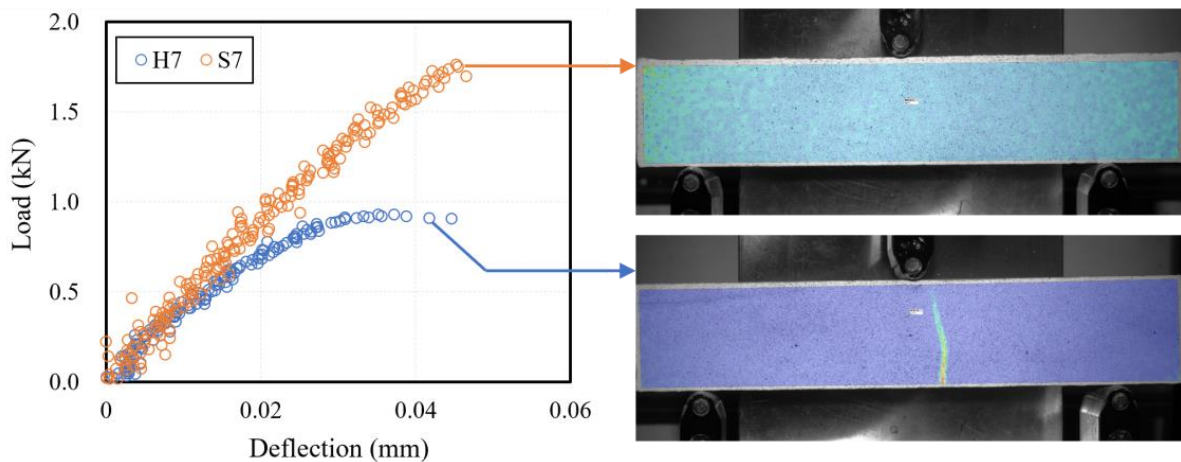


Figure 5. Penetration depth of strontium nitrate aqueous solution.

Figure 6 depicts one selected load–deflection curve from the flexural strength tests of specimens H7 and S7, along with DIC analysis images at 20 Hz showing the distribution of maximum principal stress just before failure. The maximum deflection at failure for the H7 specimen was measured to be 0.042 mm, while for the S7 specimen, it was 0.047 mm. Relative to these deflection values, a significantly higher failure load was recorded for the S7 specimen. Additionally, it was observed that specimens additionally cured in the 30% strontium nitrate solution exhibited characteristics of a brittle failure mode compared to those cured in deionized water for the same period. Initially, both H7 and S7 specimens exhibited similar load–deflection curve slopes, but after exceeding a deflection of 0.01 mm,

the slope for H7 became more gradual compared to that for S7. Furthermore, in the DIC analysis at 20 Hz, no significant change in the principal stress was detected in the S7 specimen until just before failure, whereas a clear change in the maximum principal stress was observed at the expected crack location in the H7 specimen. The results indicate that the application of a 30% strontium nitrate solution, which penetrates the surface of the specimens, alters the mechanical characteristics of the cement hydrates up to the depth of penetration, as previously mentioned. Consequently, the load–displacement curve observed in the specimen treated with strontium ions reflects a condition of a non-uniform cross-section, which is attributed to the differential modification of hydrates throughout the cross-section. Therefore, the extent of improvement in mechanical properties is influenced by factors such as the depth to which strontium ions penetrate and the dimensions of the specimen.



**Figure 6.** Flexural behavior and DIC analysis.

Figure 7a,b show the DIC analysis images for the compressive strength tests of specimens H7 and S7, respectively. These images depict the strain in the x-x direction just before failure, with red indicating areas of high strain. For the H7 specimen, a typical mode of compressive failure was observed, characterized by a 45-degree wedge fracture leading to collapse. In contrast, the S7 specimen exhibited a sudden delamination of the surface layer as a mode of failure. This difference in failure mode is attributed to the altered strength characteristics of the material up to the penetration depth, caused by the strontium nitrate solution that penetrated the specimen. Figure 7c displays the cross-section of S7, showing a penetration depth of 2 to 5 mm along the periphery. The failure occurred in the form of delamination at the boundary between the altered and unaltered regions.

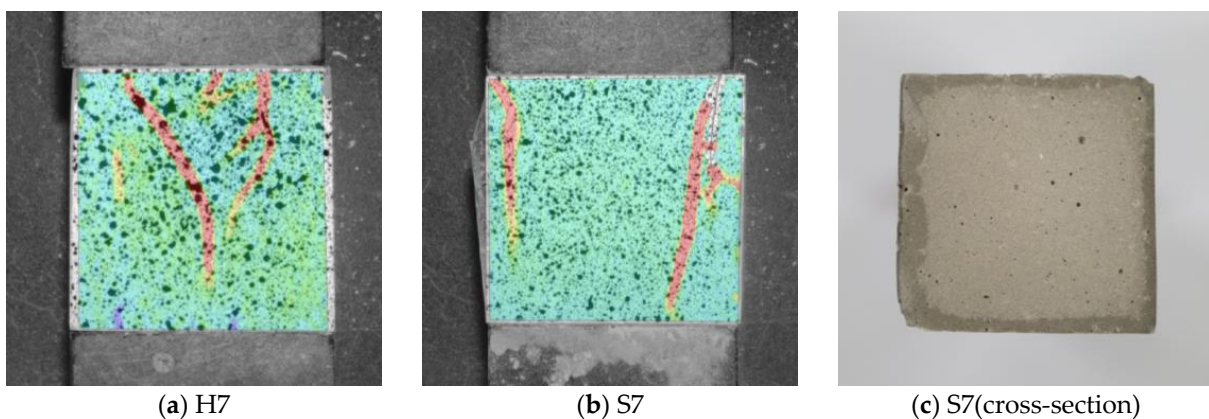


**Figure 7.** Strain analysis at compressive failure via DIC.

### 3.2. Durability Performance

Figure 8 presents the results of the surface abrasion resistance test for six different specimen IDs including the statistical analysis results. The y-axis indicates the amount of weight loss measured after the completion of the abrasion test, with smaller values representing better resistance to abrasion. It was observed that specimens treated with the 30% strontium nitrate solution showed improved surface abrasion resistance performance compared to those treated in deionized water for the same duration. The H1 specimen group exhibited an average weight loss of 1.15 g, while the S1 group recorded an average loss of 1.07 g, indicating that specimens treated for one day with the 30% strontium nitrate solution exhibited approximately 7.0% improved surface abrasion resistance performance. The S3 group (1.05 g) showed about 7.3% better performance compared to the H3 group (1.14 g), and the S7 specimens (1.04 g) recorded about 6.6% higher performance than the H7 group (1.12 g). The *p*-value ranged from 0.024 to 0.069 for the test cases, indicating that the *t*-test analysis results demonstrated a confidence level for the difference in mean values between the two groups of over 93%. Regardless of the duration of treatment with the strontium nitrate solution, a similar level of improvement in surface abrasion resistance was observed compared to the control specimens (cured in deionized water), suggesting that the performance enhancement is primarily manifested in the early stages of treatment due to the high reactivity of strontium [35].

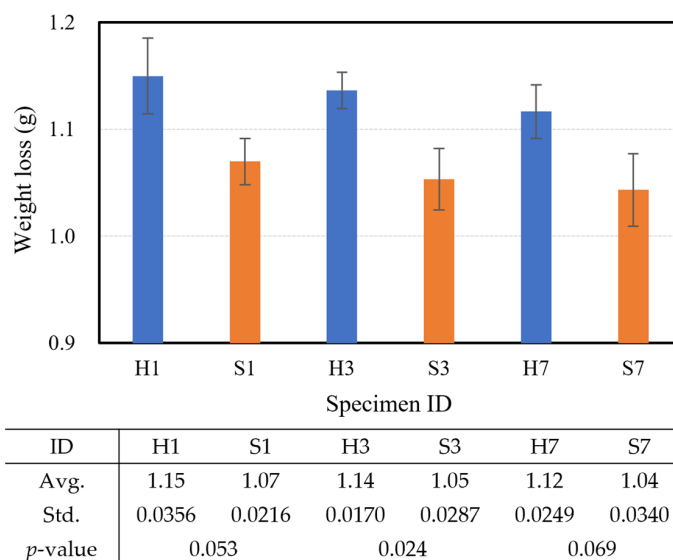


Figure 8. Results of surface abrasion resistance test.

Figure 9 presents the results of the water sorptivity test for the six different specimen groups. For each group, the average weight change due to water absorption was calculated at each measurement point up to ten days for four specimens and represented graphically. To observe the rate of water absorption at the early stage, the x-axis is represented as  $\text{day}^{0.5}$ , and the y-axis shows the weight of water absorbed through the surface of the specimen in grams (g). Water ingress occurs through the capillary pore network of the cement paste specimen, so lower values indicate greater resistance to water absorption. The results show that specimens additionally treated with the 30%  $\text{Sr}(\text{NO}_3)_2$  solution exhibited superior water absorption resistance in all cases compared to those additionally cured in deionized water for the same period. The group treated with strontium cations for 1 day (S1) showed about 9.0% improved performance compared to H1, and for the 3-day additional curing condition, S3 exhibited about 31.3% improved performance compared to H3. Furthermore, for the group treated for an additional 7 days, S7 showed about 38.0% higher water absorption resistance than H7. In other words, while strength-related characteristics were significantly manifested at the early stages of the treatment, the resistance to water

absorption increased as the duration of treatment with strontium cations lengthened. This is presumed to be due to a reduction in the distribution of capillary pores that influence water absorption as the strontium treatment period increases. Notably, the rate of water absorption in the early stages for the strontium-treated specimens (S1, S3, and S7) was significantly slower compared to the control group (H1, H3, and H7).

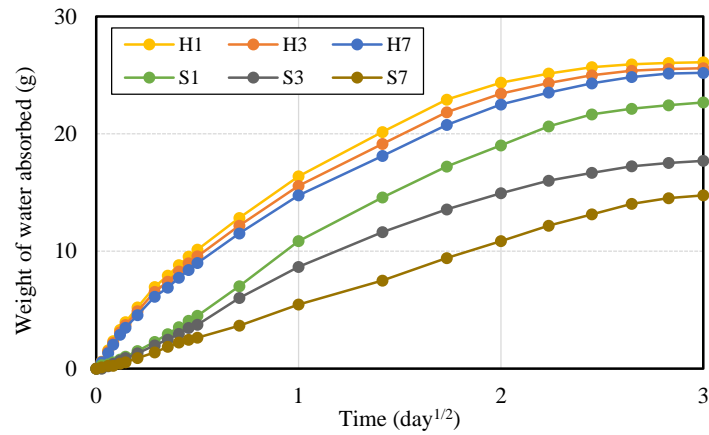
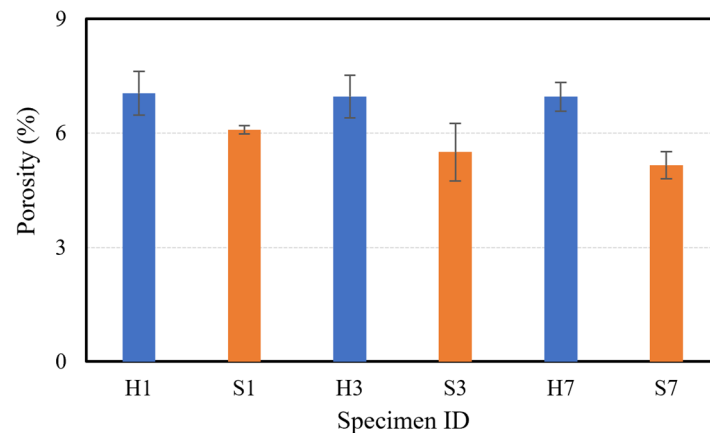


Figure 9. Results of water absorption test.

Figure 10 shows the results of the porosity measurements for the six specimen groups with the *t*-test analysis results. The average porosities for the H1 and S1 groups were 7.05% and 6.09%, respectively, indicating that a 13.7% reduction in porosity occurred due to an additional day of curing in 30% strontium nitrate solution. The S3 group, with a porosity of 5.50%, had approximately 21.0% less porosity compared to the 6.97% in the H3 group. Similarly, the porosity of the S7 group, treated with the strontium solution for 7 days, was 5.16%, which is about 25.9% lower than the 6.96% of the H7 group. In other words, while the specimen groups additionally cured in deionized water showed little change in porosity, the groups cured in the 30% strontium nitrate solution exhibited a gradual decrease in porosity over time, thereby increasing the difference compared to the control group. Moreover, the *p*-values for the testing cases exhibit very low values, indicating high reliability in the difference in average values between the treated and untreated groups. These results suggest that the treatment with strontium cations made the cement matrix denser, which is consistent with the findings from the earlier water sorptivity tests.



ID	H1	S1	H3	S3	H7	S7
Avg.	7.05	6.09	6.97	5.50	6.96	5.16
Std.	0.346	0.064	0.336	0.452	0.224	0.213
<i>p</i> -value	0.0178		0.0212		0.0012	

Figure 10. Results of porosity test.

### 3.3. Microscopic Analysis

To investigate the changes in the microstructure and chemical composition of cement hydrates due to the treatment with the 30% strontium nitrate solution, SEM and EDS analyses were conducted. These analyses aimed to examine the altered microscopic morphology of cement hydrates treated with the strontium nitrate solution over a sufficient period. The specimen S7, along with the control specimen H7, was analyzed for comparison. Specimens fractured in the flexural strength test were used for this study. A JEOL JSM-6480 SEM (JEOL, Tokyo, Japan) equipped with a 25 kV EDS was utilized in this research. Figure 11a,b, respectively, show the SEM images (magnification:  $\times 500$ ) of the H7 and S7 specimens. The structure of the specimens additionally cured in the 30% strontium nitrate solution can be visually observed to be denser compared to that of the cement paste specimens cured in deionized water for the same period. This densification is presumed to be due to the strontium nitrate solution penetrating the surface of the specimens and reacting with the already formed cement hydrates, transforming or generating different forms of hydrates. These new hydrates are believed to fill the voids, resulting in a denser structure.

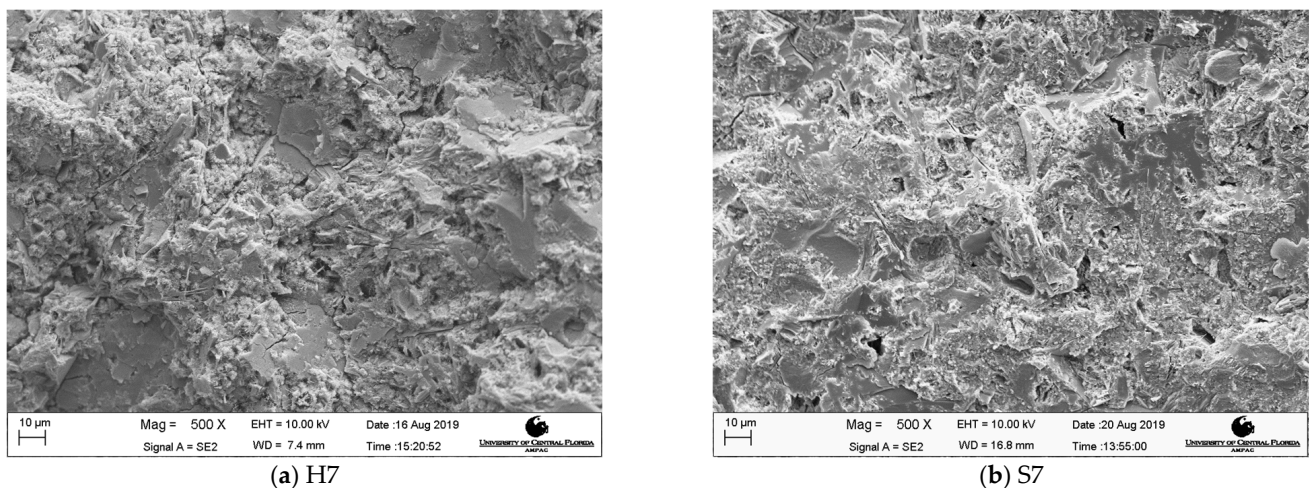


**Figure 11.** SEM analysis.

Figure 12 shows the results of EDS analyses conducted on six different areas of the S7 specimen. Areas that appeared to differ from the typical components of cement hydrates were selected for EDS analysis, and the atomic percentages of five elements (O, Si, Ca, Al, Sr) were analyzed. As shown in the analysis results, the Sr element was detected in all areas. Areas 1, 3, and 5, with almost no aluminum element, are presumed to be primarily altered C-S-H hydrates, while areas 2, 4, and 6 are believed to be hydrates formed from reactions between the strontium and the aluminum-containing cement hydrates, such as C-A-S-H (calcium aluminosilicate hydrate), AFm, and Aft. Additionally, the typical needle-like appearance of the AFm and CH hydrates, commonly found in normally cured hydrated cement composites, was hardly observed. Figure 13 presents the results of EDS element mapping analysis for the S7 specimen. Figure 13a shows the analyzed specimen, with the left end being the surface where the strontium nitrate solution penetrated, and penetration progressing towards the right, analyzed up to a depth of approximately 5 mm. Figure 13b,c, respectively, show the distributions of calcium and strontium elements. It was observed that the concentration of strontium increases closer to the surface of the specimen, while the concentration of calcium decreases. Strontium elements were detected throughout the analyzed depth (i.e., up to 5 mm beneath the surface).

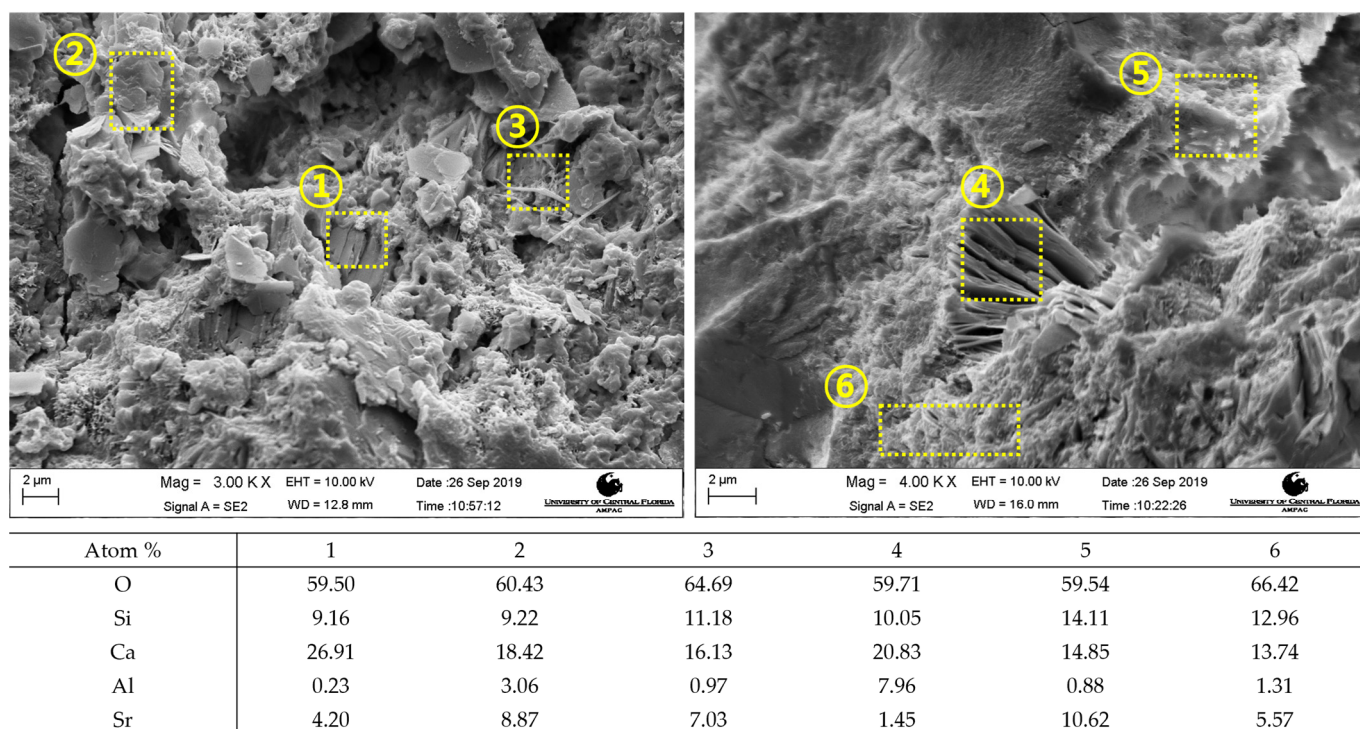


Figure 12. EDS analysis.

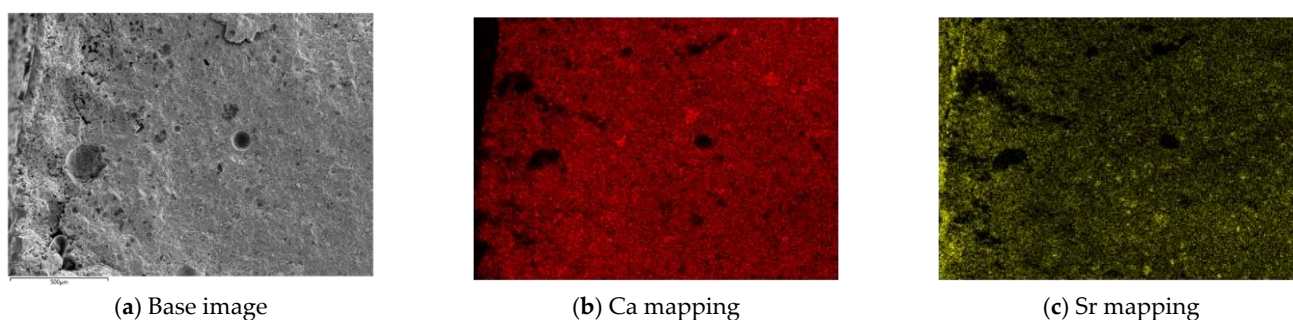


Figure 13. EDS mapping analysis.

XRD analysis was conducted to investigate the crystalline phase changes in a hydrated cement matrix upon interaction with strontium nitrate solution. For this study, a Rigaku D/MAX XRD II was utilized, performing 2-theta scanning from  $5^\circ$  to  $80^\circ$  with a step size of  $0.02^\circ$ , in accordance with ASTM C295 [36]. Three samples were prepared for the XRD analysis to identify phase changes over time: a hydrated cement paste cured for 28 days in deionized water, S3, and S7. Each sample was ground into powder prior to the analysis. The results are shown in Figure 14. A decrease in the relative peak intensities of  $\text{Sr}(\text{NO}_3)_2$  at specific  $2\theta$  degrees over time was observed, indicating its consumption within the hydrated cement matrix. This was particularly evident in the comparison of samples S3 and S7, supporting the hypothesis of  $\text{Sr}(\text{NO}_3)_2$ 's active involvement in the chemical reactions within the matrix. Subsequently, the amount of portlandite ( $\text{Ca}(\text{OH})_2$ ) was found to have dramatically diminished after the treatment, as observed in S3 and S7. This suggests the consumption of  $\text{Ca}(\text{OH})_2$  in the formation of new hydrates, possibly involving strontium. Moreover, the formation of different types of zeolite structures, including zeolite Barrer L-Sr and clinoptilolite, was identified, indicating the conversion of aluminates hydrates into zeolites with varying silicon content and cation exchange capabilities. A similar trend to the result reported in a previous study [27] is shown with these results.

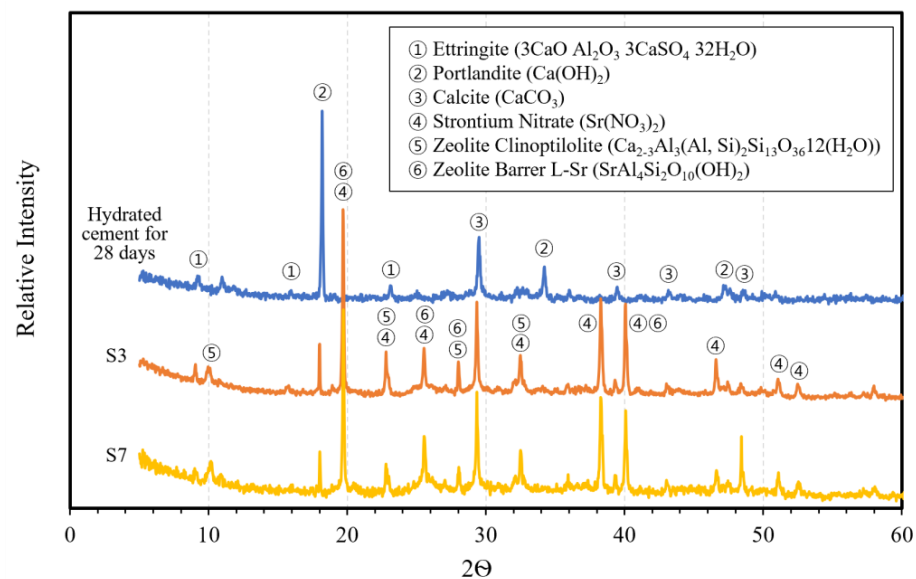


Figure 14. XRD analysis.

#### 4. Conclusions

This study examined the potential of post-hardening treatment using  $\text{Sr}^{2+}$  for modifying the properties of hydrated cement composites. The effects of treatment with a 30% strontium nitrate aqueous solution on the strength characteristics of cement composites were investigated. Additionally, durability aspects such as surface abrasion resistance, water sorptivity, and porosity were evaluated in the cement paste specimens treated with the strontium nitrate solution. Microscopic morphology changes in the hardened cement hydrates due to strontium cations were analyzed using SEM, EDS, and XRD. Based on the testing results, the following conclusions can be drawn:

Treating hardened cement paste composites with a 30% strontium nitrate solution enhanced both compressive and flexural strengths. Notably, flexural strength showed a remarkable improvement, with over 70% enhancement in early stage strontium-treated specimens compared to those cured in deionized water for the same period.

The penetration of the 30% strontium nitrate solution into the 28-day cured cement paste specimens reached up to 6.5 mm over an additional 7 days. Most penetration appears to occur in the early stages of the treatment process. This penetration likely alters the hydrated cement components into new forms, contributing to the observed strength enhancements.

Specimens treated with the strontium showed improved surface abrasion resistance and reduced water absorption. Additionally, a significant reduction in porosity was noted in the strontium-treated specimens. These results led to enhanced surface durability, suggesting a denser and more durable surface layer. The strontium treatment process rapidly improved the surface abrasion resistance characteristics, while porosity and water sorptivity gradually decreased over time.

SEM, EDS, and XRD analyses revealed a denser microstructure in the hydrated cement paste composites and confirmed the presence of strontium throughout the treated layer. New hydrate shapes, not typically found in normal hydrated cement composites, were identified and are believed to be formed by strontium. Several types of zeolite structures were identified, accompanied by an observed decrease in the portlandite phase. These changes are thought to be responsible for the improved mechanical and durability performance of the strontium-treated specimens.

In conclusion, treatment with strontium cations offers a promising approach for enhancing the durability of hydrated cement composites post-hardening, along with improved mechanical characteristics. This highlights the potential of strontium cation treatment in extending the service life of cement concrete structures.

**Funding:** This research was funded by 2021 and 2022 Research Grants from Sangmyung University (2021-A000-0011 and 2022-A000-0099).

**Institutional Review Board Statement:** Not applicable.

**Informed Consent Statement:** Not applicable.

**Data Availability Statement:** Data are available from the authors upon reasonable request.

**Conflicts of Interest:** The authors declare no conflict of interest.

## References

- Alnahhal, M.F.; Alengaram, U.J.; Jumaat, M.Z.; Alsubari, B.; Alqedra, M.A.; Mo, K.H. Effect of aggressive chemicals on durability and microstructure properties of concrete containing crushed new concrete aggregate and non-traditional supplementary cementitious materials. *Constr. Build. Mater.* **2018**, *163*, 482–495. [\[CrossRef\]](#)
- Roesler, J.R.; Cervantes, V.G.; Amirkhanian, A.N. Accelerated performance testing of concrete pavement with short slabs. *Int. J. Pavement Eng.* **2012**, *13*, 494–507. [\[CrossRef\]](#)
- Sajid, H.U.; Jalal, A.; Kiran, R.; Al-Rahim, A. A survey on the effects of deicing materials on properties of Cement-based materials. *Constr. Build. Mater.* **2022**, *319*, 126062. [\[CrossRef\]](#)
- Liu, J.; Zhang, W.; Li, Z.; Jin, H.; Tang, L.J.C.; Materials, B. Influence of deicing salt on the surface properties of concrete specimens after 20 years. *Constr. Build. Mater.* **2021**, *295*, 123643. [\[CrossRef\]](#)
- Gan, Y.; Li, C.; Ke, W.; Deng, Q.; Yu, T. Study on pavement performance of steel slag asphalt mixture based on surface treatment. *Case Stud. Constr. Mater.* **2022**, *16*, e01131. [\[CrossRef\]](#)
- Zhang, Z.; Zhang, H.; Lv, J.; Li, W. Performance evaluation of skid-resistant surface treatment using lithium silicate for limestone bituminous pavement. *Constr. Build. Mater.* **2022**, *342*, 127990. [\[CrossRef\]](#)
- Zhang, Z.; Luan, B.; Liu, X.; Zhang, M. Effects of surface texture on tire-pavement noise and skid resistance in long freeway tunnels: From field investigation to technical practice. *Appl. Acoust.* **2020**, *160*, 107120. [\[CrossRef\]](#)
- Ryu, S.; Kim, J.; Sohn, D.; Bae, S. Optimal longitudinal texture on concrete pavement to reduce lateral vibration of vehicles. *Appl. Sci.* **2022**, *12*, 9661. [\[CrossRef\]](#)
- Zhao, Z.; Qu, X.; Li, J. Application of polymer modified cementitious coatings (PCCs) for impermeability enhancement of concrete. *Constr. Build. Mater.* **2020**, *249*, 118769. [\[CrossRef\]](#)
- Zhang, P.; Wang, W.; Lv, Y.; Gao, Z.; Dai, S. Effect of polymer coatings on the permeability and chloride ion penetration resistances of nano-particles and fibers-modified cementitious composites. *Polymers* **2022**, *14*, 3258. [\[CrossRef\]](#)
- Li, J.; Yi, Z.; Xie, Y. Progress of silane impregnating surface treatment technology of concrete structure. *Mater. Rev.* **2012**, *26*, 120–125.
- Xiong, B.B.; Gao, L.; Chen, J.G.; Lu, X.C.; Tian, B.; Chen, B.F.; Li, Y.B. Action mechanism for improving water impermeability of concrete surface based on deep penetrating sealer. *Constr. Build. Mater.* **2022**, *322*, 126424. [\[CrossRef\]](#)
- Dong, Q.; Cao, X.; Wang, S.; Chen, X.; Yang, B.; Xie, S.; Cheng, Z. Design and Evaluation of an Innovative Composite Silicate-based Surface Treatment Agent of Concrete. *Case Stud. Constr. Mater.* **2023**, *18*, e02207. [\[CrossRef\]](#)
- Herath, C.; Gunasekara, C.; Law, D.W.; Setunge, S. Performance of high volume fly ash concrete incorporating additives: A systematic literature review. *Constr. Build. Mater.* **2020**, *258*, 120606. [\[CrossRef\]](#)
- Villain, G.; Platret, G. Two experimental methods to determine carbonation profiles in concrete. *ACI Mater. J.* **2006**, *103*, 265.
- Atkins, M.; Glasser, F.P. Application of Portland cement-based materials to radioactive waste immobilization. *Waste Manag.* **1992**, *12*, 105–131. [\[CrossRef\]](#)
- Zhu, Y.; Zheng, Z.; Deng, Y.; Shi, C.; Zhang, Z. Advances in immobilization of radionuclide wastes by alkali activated cement and related materials. *Cem. Concr. Compos.* **2022**, *126*, 104377. [\[CrossRef\]](#)
- Panpisut, P.; Liaqat, S.; Zacharaki, E.; Xia, W.; Petridis, H.; Young, A.M. Dental composites with calcium/strontium phosphates and polylysine. *PLoS ONE* **2016**, *11*, e0164653. [\[CrossRef\]](#)
- Meunier, P.J.; Roux, C.; Seeman, E.; Ortolani, S.; Badurski, J.E.; Spector, T.D.; Cannata, J.; Balogh, A.; Lemmel, E.-M.; Pors-Nielsen, S. The effects of strontium ranelate on the risk of vertebral fracture in women with postmenopausal osteoporosis. *N. Engl. J. Med.* **2004**, *350*, 459–468. [\[CrossRef\]](#)
- Reginster, J.-Y.; Seeman, E.; De Vernejoul, M.; Adami, S.; Compston, J.; Phenekos, C.; Devogelaer, J.-P.; Curiel, M.D.; Sawicki, A.; Goemaere, S. Strontium ranelate reduces the risk of nonvertebral fractures in postmenopausal women with osteoporosis: Treatment of Peripheral Osteoporosis (TROPOS) study. *J. Clin. Endocrinol. Metab.* **2005**, *90*, 2816–2822. [\[CrossRef\]](#)
- Schumacher, M.; Henß, A.; Rohnke, M.; Gelinsky, M. A novel and easy-to-prepare strontium (II) modified calcium phosphate bone cement with enhanced mechanical properties. *Acta Biomater.* **2013**, *9*, 7536–7544. [\[CrossRef\]](#) [\[PubMed\]](#)
- Shiner, M.E.; Klein-BenDavid, O.; L'Hôpital, E.; Dauzères, A.; Neji, M.; Teutsch, N.; Bar-Nes, G. Retention of strontium in high- & low-pH cementitious matrices-OPC vs. model systems. *Cem. Concr. Res.* **2022**, *152*, 106659.
- Wieland, E.; Tits, J.; Kunz, D.; Dähn, R. Strontium uptake by cementitious materials. *Environ. Sci. Technol.* **2008**, *42*, 403–409. [\[CrossRef\]](#) [\[PubMed\]](#)

24. Tits, J.; Wieland, E.; Müller, C.J.; Landesman, C.; Bradbury, M.H. Strontium binding by calcium silicate hydrates. *J. Colloid Interface Sci.* **2006**, *300*, 78–87. [[CrossRef](#)] [[PubMed](#)]
25. Tomita, S.; Haga, K.; Hosokawa, Y.; Yamada, K.; Igarashi, G.; Maruyama, I. Modeling of the adsorption behavior of Cs and Sr on calcium silicate hydrates. *J. Adv. Concr. Technol.* **2021**, *19*, 1061–1074. [[CrossRef](#)]
26. Iwaida, T.; Nagasaki, S.; Tanaka, S. Sorption study of strontium onto hydrated cement phases using a sequential desorption method. *Radiochim. Acta* **2000**, *88*, 483–487. [[CrossRef](#)]
27. Cho, B.H.; Nam, B.H.; Santra, S.; Barry, M.; Novak, S. Enhanced surface hardening of hydrated concrete composite by strontium nitrate ( $\text{Sr}(\text{NO}_3)_2$ ) aqueous solution. *J. Build. Eng.* **2021**, *40*, 102696. [[CrossRef](#)]
28. Winslow, D.N.; Dolch, W.L. Cement paste hydrated in  $\text{Sr}(\text{OH})_2$ . *Cem. Concr. Res.* **1976**, *6*, 309–319. [[CrossRef](#)]
29. *ASTM-C150*; Standard Specification for Portland Cement. ASTM International: West Conshohocken, PA, USA, 2018.
30. *ASTM-C109*; Standard Test Method for Compressive Strength of Hydraulic Cement Mortars. ASTM International: West Conshohocken, PA, USA, 2016.
31. *ASTM-C293*; Standard Test Method for Flexural Strength of Concrete (Using Simple Beam with Center-Point Loading). ASTM International: West Conshohocken, PA, USA, 2016.
32. Sutton, M.A.; Wolters, W.J.; Peters, W.H.; Ranson, W.F.; McNeill, S.R. Determination of displacements using an improved digital correlation method. *Image Vis. Comput.* **1983**, *1*, 133–139. [[CrossRef](#)]
33. *ASTM-C1585*; Standard Test Method for Measurement of Rate of Absorption of Water by Hydraulic-Cement Concretes. ASTM International: West Conshohocken, PA, USA, 2013.
34. *ASTM-C1754*; Standard Test Method for Density and Void Content of Hardened Pervious Concrete. ASTM International: West Conshohocken, PA, USA, 2012.
35. Faure, G.; Powell, J.L. *Strontium Isotope Geology*; Springer Science & Business Media: Berlin, Germany, 2012; Volume 5.
36. *ASTM-C295/C295M-18*; Standard Guide for Petrographic Examination of Aggregates for Concrete. ASTM International: West Conshohocken, PA, USA, 2018.

**Disclaimer/Publisher’s Note:** The statements, opinions and data contained in all publications are solely those of the individual author(s) and contributor(s) and not of MDPI and/or the editor(s). MDPI and/or the editor(s) disclaim responsibility for any injury to people or property resulting from any ideas, methods, instructions or products referred to in the content.